AGU PUBLICATIONS

JGR

Journal of Geophysical Research: Biogeosciences

RESEARCH ARTICLE

10.1002/2015JG003047

Key Points:
- Both gas transport and heat flow can introduce [CO_2]-Ts and Rs-Ts hystereses
- Areas of [CO_2]-Ts and Rs-Ts correlate with soil moisture in an opposite way
- Stimulation of photosynthesis can produce 8-shaped hysteresis

Supporting Information:
- Figures S1 – S4 and Table S1

Correspondence to:
Q. Zhang,
quan.zhang@whu.edu.cn

Citation:
Zhang, Q., G. G. Katul, R. Oren, E. Daly, S. Manzoni, and D. Yang (2015), The hysteresis response of soil CO_2 concentration and soil respiration to soil temperature, *J. Geophys. Res. Biogeosci.*, *120*, doi:10.1002/2015JG003047.

Received 6 MAY 2015
Accepted 16 JUL 2015
Accepted article online 20 JUL 2015

The hysteresis response of soil CO_2 concentration and soil respiration to soil temperature

Quan Zhang[1,2,3], Gabriel G. Katul[3,4], Ram Oren[3], Edoardo Daly[5], Stefano Manzoni[6,7], and Dawen Yang[2]

[1]State Key Laboratory of Water Resources and Hydropower Engineering Science, College of Water Resources and Hydropower Engineering, Wuhan University, Wuhan, China, [2]State Key Laboratory of Hydroscience and Engineering, Department of Hydraulic Engineering, Tsinghua University, Beijing, China, [3]Nicholas School of the Environment, Duke University, Durham, North Carolina, USA, [4]Department of Civil and Environmental Engineering, Duke University, Durham, North Carolina, USA, [5]Department of Civil Engineering, Monash University, Clayton, Victoria, Australia, [6]Department of Physical Geography, Stockholm University, Stockholm, Sweden, [7]Bolin Center for Climate Research, Stockholm University, Stockholm, Sweden

Abstract Diurnal hysteresis between soil temperature (T_s) and both CO_2 concentration ([CO_2]) and soil respiration rate (R_s) were reported across different field experiments. However, the causes of these hysteresis patterns remain a subject of debate, with biotic and abiotic factors both invoked as explanations. To address these issues, a CO_2 gas transport model is developed by combining a layer-wise mass conservation equation for subsurface gas phase CO_2, Fickian diffusion for gas transfer, and a CO_2 source term that depends on soil temperature, moisture, and photosynthetic rate. Using this model, a hierarchy of numerical experiments were employed to disentangle the causes of the hysteretic [CO_2]-T_s and CO_2 flux T_s (i.e., F-T_s) relations. Model results show that gas transport alone can introduce both [CO_2]-T_s and F-T_s hystereses and also confirm prior findings that heat flow in soils lead to [CO_2] and F being out of phase with T_s, thereby providing another reason for the occurrence of both hystereses. The area (A_{hys}) of the [CO_2]-T_s hysteresis near the surface increases, while the A_{hys} of the R_s-T_s hysteresis decreases as soils become wetter. Moreover, a time-lagged carbon input from photosynthesis deformed the [CO_2]-T_s and R_s-T_s patterns, causing a change in the loop direction from counterclockwise to clockwise with decreasing time lag. An asymmetric 8-shaped pattern emerged as the transition state between the two loop directions. Tracing the pattern and direction of the hysteretic [CO_2]-T_s and R_s-T_s relations can provide new ways to fingerprint the effects of photosynthesis stimulation on soil microbial activity and detect time lags between rhizospheric respiration and photosynthesis.

1. Introduction

The CO_2 efflux from the soil surface (hereafter soil respiration R_s), which represents one of the largest terrestrial CO_2 sources to the atmosphere [*Raich and Schlesinger*, 1992], is controlled by numerous factors, including soil temperature (T_s) [e.g., *Lloyd and Taylor*, 1994; *Risk et al.*, 2002], soil moisture (θ) [e.g., *Davidson et al.*, 2000; *Daly et al.*, 2008; *Manzoni et al.*, 2012], photosynthesis [e.g., *Tang et al.*, 2005; *Vargas and Allen*, 2008a; *Zhang et al.*, 2013], soil organic carbon (SOC) content [e.g., *Wan and Luo*, 2003], nutrient addition [e.g., *Janssens et al.*, 2010], and carbon allocation by plants [e.g., *Palmroth et al.*, 2006]. Among these factors, T_s is generally considered the most dynamic and is used in the majority of R_s models [*Lloyd and Taylor*, 1994; *Daly et al.*, 2009; *Zhang et al.*, 2013], often in the form of a Q_{10} expression. With automation in R_s measurements and the need to resolve diurnal variability when quantifying net ecosystem exchange of CO_2 with the atmosphere, the R_s-T_s variations at hourly time scales is receiving significant attention. It became apparent from several experiments that during the course of a single day, a hysteretic relation emerges between soil respiration and soil temperature measured at some depth z from the soil surface (Table 1). Such hysteresis cycles between R_s and soil temperature are not represented in the current Q_{10} expressions used in virtually all large-scale models, prompting interest in the causes of the hysteresis and the resulting errors in the estimation of soil respiration fluxes when ignoring this hysteretic effect [*Oikawa et al.*, 2014]. The purpose of this work is to investigate the mechanism driving such hysteresis.

Table 1. Observed Diurnal Hysteresis of Soil [CO_2] and R_s with Soil Temperature

Measured Quantity[a]	Method[b]	Loop Direction[c]	Suggested Drivers[d]	Magnitude[e]	Plant Type or Species[f]	Source
[CO_2]	GMP221	1 8	θ	H_w	bluejoint reedgrass	*Riveros-Iregui et al.* [2007]
S	GC	1	NA	NA	spruce, cedar, sedge in peat	*Updegraff et al.* [1998]
R_s	DCS	1 8[g]	NA	NA	corn, soybean	*Parkin and Kaspar* [2003]
R_s	GMT222	2	NA	NA	oak-grass savanna	*Tang et al.* [2005]
R_s	DCS	1 2	rhizospheric respiration	NA	boreal trembling aspen	*Gaumont-Guay et al.* [2006]
R_s	DCS	1 8	τ, photosynthesis	NA	pasture	*Bahn et al.* [2008]
R_s	DCS	1	NA	NA	grass, shrub	*Carbone et al.* [2008]
R_s	GMT222	1 2	NA	NA	forest with 53 tree species	*Vargas and Allen* [2008a]
R_s	GMM222	1 8	τ, photosynthesis	NA	conifers, oak	*Vargas and Allen* [2008b]
R_s	GMM220	1	NA	NA	conifers, oak	*Vargas and Allen* [2008c]
R_s	GMP343	1 2	NA	RMSE	peanut[h]	*Pingintha et al.* [2010]
R_s	DCS	2	NA	H_w[i]	oak, maple, pine, hemlock	*Phillips et al.* [2010]
R_s	DCS	1 2	τ	NA	mixed forest of beach, ash, fir, etc	*Ruehr et al.* [2010]
R_s	NA	1 2	NA	NA	NA	*Subke and Bahn* [2010]
R_s	DCS[j]	1	NA	NA	grass, woody shrubs and trees	*Thomas and Hoon* [2010]
R_s	GMT222	2	θ, τ, photosynthesis	DMT	velvet mesquite, bunchgrass	*Barron-Gafford et al.* [2011]
R_s	GMT222	1[k] 2[l]	NA	NA	cotton	*Li et al.* [2011]
R_s	NA	1 2	τ	R^2	NA	*Phillips et al.* [2011]
R_s	DCS	1	NA	NA	wheat, potato, beet, *Douglas fir*, beeches[m]	*Buysse et al.* [2013]
R_s	DCS	1 8	NA	NA	*Pinus tabulaeformis*	*Jia et al.* [2013]
R_s	DCS	1	NA	NA	korshinsk peashrub, leguminous herb, fallow, millet	*Fu et al.* [2013]
R_s	DCS	1[n] 2[o]	τ	NA	*Quercus rubra*, *Acer rubrum*	*Savage et al.* [2013]
R_s	GMT220	1 2	τ, photosynthesis	DMT	*Sorghum bicolor*	*Oikawa et al.* [2014]
R_s	DCS	1[p]	θ, photosynthesis	NA	*Artemisia ordosical*, *Hedysarum mongolicum*	*Wang et al.* [2014]
R_s	DCS	NA	τ	R^2	7 forests in the Amazon basin	*Zanchi et al.* [2014]

[a] [CO_2] denotes CO_2 concentration, S denotes soil CO_2 production, R_s denotes soil respiration (i.e., near-surface CO_2 efflux).

[b] GMP221, GMP343, GMT220, GMT222, GMM220, and GMM222 denote the types of carbon dioxide probes for [CO_2] measurements, respectively, R_s is therefore calculated based on gas gradient method applied in this study; GC denotes gas chromatograph method; DCS denotes dynamic closed system containing an Infra-Red Gas Analyzer (IRGA) and a chamber, including the commonly used commercial LI-8100, LI-8100A, and LI-6400 systems and other self-made systems; NA means no field measurements were conducted, and numerical methods were used to generate R_s.

[c] 1 denotes clockwise, 2 denotes counterclockwise, 8 denotes an eight-shaped pattern, NA means no direction was suggested, nor was there sufficient information to derive the direction.

[d] Suggested factors were summarized into three types, i.e., soil moisture (θ); biological controls of photosynthesis, rhizoshperic respiration, and root activity; and time lag (τ) between R_s and soil temperature (induced by soil heat flow), lag between photosynthesis and root CO_2 production, soil CO_2 diffusion, etc. NA means no clear factor is proposed or no strong evidence supporting any factors.

[e] H_w denotes width; RMSE (originally presented as "residual values" calculated as the difference between measured and modeled values in *Pingintha et al.* [2010]; we speculate that it is equivalent to RMSE) denotes the error (i.e., root-mean-square error) between measured and modeled R_s by the fitting temperature response curve; DMT denotes the Difference at Median Temperature; R^2 denotes the determination coefficient for the performance of fitting the temperature response curve of R_s; NA means no value was proposed or used to quantify the hysteresis magnitude.

[f] NA means that R_s was obtained from mathematical calculation; therefore, there is no plant type.

[g] The "8"-shaped pattern occurs in the relation between R_s and air temperature.

[h] Plants were removed, the site was therefore bare soil containing root residual.

[i] The width here is different from its common definition, as this study calculates the direct residual range based on the linear regression.

[j] The [CO_2] was determined by gas chromatograph instead of the commonly used IRGA.

[k] Both hystereses of the heterotrophic respiration and total respiration with respect to temperature were clockwise.

[l] The hysteresis of autotrophic respiration versus soil temperature was counterclockwise.

[m] Soil was collected for soil CO_2 production measurement, thus, R_s only includes heterotrophic respiration.

[n] Hysteresis of heterotrophic respiration versus soil temperature was clockwise.

[o] Hysteresis of total respiration versus soil temperature was counterclockwise.

[p] R_s peaked earlier than soil temperature, therefore resulting in clockwise hysteresis.

A plausible argument for the onset of this hysteretic R_s-T_s relation is the presence of time lags between measurements of R_s at the soil surface and the conditions contributing to investigate to such a flux at a certain soil depth z below the surface. Specifically, T_s, θ, and carbon (C) inputs from roots drive CO_2 production locally at z, but the transport of CO_2 to the surface causes delays in the observed respiration rate. Even the CO_2 flux ($F(z)$) and the environmental conditions at the same depth can be out of phase, since the flux integrates sources from other depths, causing hysteretic loops. There are other lags such as the lag between microbial activation and T_s, though such lags are commonly assumed to be short (< 60 s) with respect to the averaging period used in the analysis of R_s and T_s (≈ 3600 s), as discussed in *Jones and Murphy* [2007]. Delays between CO_2 efflux and temperature at the source are undisputed [*Bahn et al.*, 2008; *Phillips et al.*, 2011; *Zanchi et al.*, 2014], reasonably understood, and supported by prior model results [*Phillips et al.*, 2011]. In fact, significant amount of prior work did focus on the measured hysteretic relation between R_s (i.e., $F(0)$) and T_s at some arbitrary depth (e.g., $z = 2, 5, 10$ cm). The consequences of this arbitrary choice of a T_s depth on the R_s-T_s hysteresis is known to introduce artificial hysteresis.

Soil moisture was also conjectured to control hysteresis between R_s and T_s in some studies [*Ruehr et al.*, 2010; *Wang et al.*, 2014], but not in other studies [*Tang et al.*, 2005; *Pingintha et al.*, 2010]. The different roles of soil moisture may be due to the fact that the depth-integrated soil moisture does not vary appreciably during a single day, while rhizosphere soil moisture (or water potential) may change far more appreciably, thereby regulating soil CO_2 production and gas diffusion. Photosynthesis was also proposed as one controlling variable on soil respiration [*Kuzyakov and Cheng*, 2001; *Tang et al.*, 2005; *Stoy et al.*, 2007; *Zhang et al.*, 2013] and was suggested to be partly responsible for the observed R_s-T_s hysteresis [e.g., *Tang et al.*, 2005; *Bahn et al.*, 2008; *Carbone et al.*, 2008; *Vargas and Allen*, 2008b; *Savage et al.*, 2013; *Oikawa et al.*, 2014; *Wang et al.*, 2014]. Measurements reporting the absence of R_s-T_s hysteresis in soils without plants support this hypothesis [*Oikawa et al.*, 2014]. However, hysteresis patterns reported in root-free conditions at other sites [*Pingintha et al.*, 2010] challenge this conclusion. These contrasting results point to a limited understanding of the effects of photosynthesis on the R_s-T_s hysteresis the subject of the analysis here.

The aforementioned mechanisms typically lead to a hysteretic R_s-T_s relation characterized by a closed elliptic-shaped loop pattern. Other patterns in R_s-T_s relation have also been reported. An 8-shaped R_s-T_s relation was reported [*Parkin and Kaspar*, 2003; *Bahn et al.*, 2008; *Barron-Gafford et al.*, 2011; *Jia et al.*, 2013], but these interesting patterns were rarely discussed (Table 1). The occurrence of such 8-shaped pattern implies that compound-controlling factors are at play and disentangling them is part of the scope here.

In parallel to the well-studied hysteretic R_s-T_s relation, a soil $[CO_2]$-T_s hysteresis was reported in some studies on diurnal time scales. *Riveros-Iregui et al.* [2007] suggested that diurnal $[CO_2]$-T_s hysteresis might be controlled by θ. Their argument rests on the assumption that rhizodeposition and its breakdown increases with higher θ resulting in soil $[CO_2]$-T_s hysteresis of larger magnitude. Similar to the 8-shaped R_s-T_s pattern, different hysteresis patterns ranging from the conventional elliptic shape to 8 shape are evident in the $[CO_2]$-T_s relations reported in *Riveros-Iregui et al.* [2007] (but the 8-shaped pattern was not discussed). The 8-shaped $[CO_2]$-T_s pattern, for example, appeared in field measurements across several depths in a pine forest discussed here (Figure 1), implying that the 8-shaped $[CO_2]$-T_s relation may be more ubiquitous than previously considered.

Despite many field experiments and numerical results providing partial explanations to the occurrence of the hysteresis [e.g., *Phillips et al.*, 2011], studies based on the combined use of models and observations remain rare, leaving a number of unanswered questions on the R_s-T_s and $[CO_2]$-T_s hystereses: (1) What are the main causes of the hysteretic $[CO_2]$-T_s and R_s-T_s relations? (2) How do we reconcile inconsistencies in the role of θ on the hysteretic R_s-T_s relation? (3) How does photosynthesis regulate the hysteretic R_s-T_s and the $[CO_2]$-T_s relations and how is photosynthesis linked to the aforementioned 8-shaped pattern? (4) At a more fundamental level, what are the connections between the shapes of the R_s-T_s and the $[CO_2]$-T_s hystereses? These questions motivate the present work, where plausible explanations are assessed using a one-dimensional model of soil gas phase CO_2 transport complemented with field $[CO_2]$ measurements.

2. Materials and Methods

2.1. Data Description

The field experiments were conducted in 2005 and 2006 in a Southeastern Loblolly Pine (*Pinus taeda* L.) plantation situated within the Blackwood Division of the Duke Forest, near Durham, North Carolina, USA

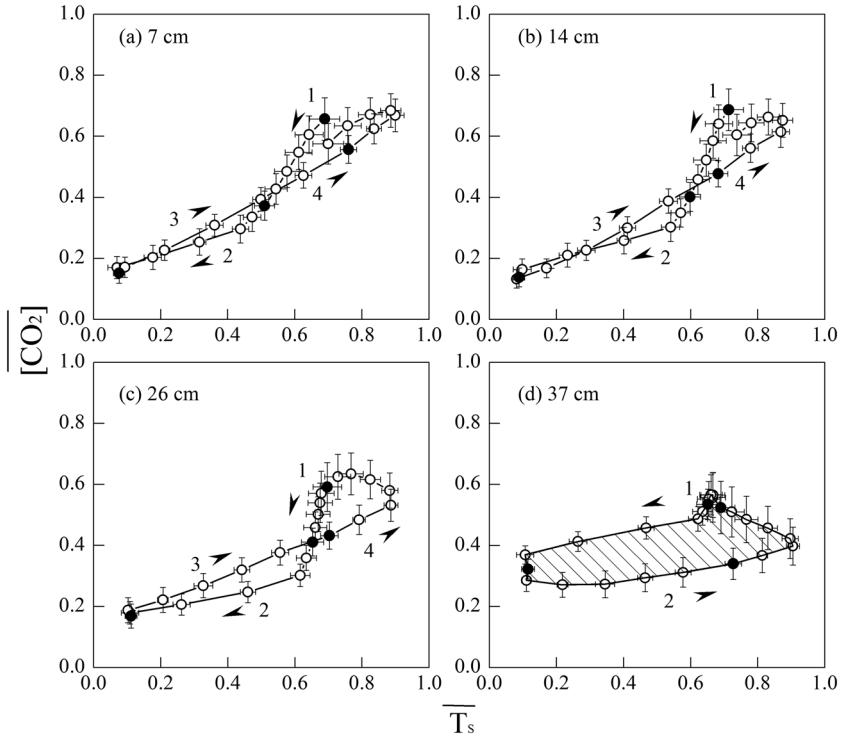

Figure 1. Ensemble-averaged hysteresis of normalized soil $[CO_2]$ ($\overline{[CO_2]}$) and soil temperature ($\overline{T_S}$) for (a–d) different soil layers (labeled by the $[CO_2]$ collected depth) at one location in a Southern Loblolly Pine (*Pinus taeda* L.) stand near Durham, North Carolina, USA. The ensemble diurnal hysteresis of $[CO_2]$ and T_S was obtained by normalizing with a reference daily maximum and minimum and averaging hour by hour over a 30 day period commencing from 1 March 2006 (i.e., $\overline{x} = (x - x_{min})/(x_{max} - x_{min})$, where $\overline{x}$ denotes normalized soil $[CO_2]$ or temperature, and x_{min} and x_{max} denote daily minimum and maximum, respectively). Horizontal and vertical lines indicate 1 standard error around the monthly mean. Note that measured T_s in Figure 1b is taken from $z = 16$ cm, in Figure 1c from $z = 28$ cm, and in Figure 1d from $z = 38$ cm. Numbers and arrows (here and hereafter) indicate the progression of the diurnal cycle starting from midnight. The filled circles close to number 1 denote midnight (0:00), while the other filled circles denote 6:00, 12:00 (noon), and 18:00. The hatched area in Figure 1d shows the area enveloped by the hysteresis loop A_{hys}, used as a measure of hysteresis magnitude.

(35°58′N,79°08′W). Profiles of gas phase soil CO_2 concentration at $z = 7$, 14, 26, 37, and 45 cm below the soil surface were collected using solid state infrared CO_2 transmitters (GMT 221 model, Vaisala, Finland). These concentration profiles were complemented by T_s measurements collected at $z = 7$, 16, 21, 28, and 38 cm below the soil surface using thermocouples (105T-L16, Campbell Scientific Inc., Logan, Utah, USA), and by θ measurements collected at $z = 3$, 6, 16, 21, and 39 cm using Theta Probes (model ML2x, Delta-T Devices, Cambridge, UK). These data were selected from one of the Free Air CO_2 Enrichment (FACE) experiment sites [*Daly et al.*, 2009] primarily due to data continuity in T_s, θ, gas phase soil $[CO_2]$, and eddy covariance CO_2 record in ambient conditions ($[CO_2] = 380$ ppm), rather than due to a particular field treatment. The soil $[CO_2]$ measurements were temperature corrected as described in *Daly et al.* [2009]. Soil surface CO_2 efflux was measured using the Automated Carbon Efflux System (ACES, USDA Forest Service, US Patent 6,692,970)—that employs an IRGA (Infra-Red Gas Analyzer)-based open system. Measurements of four plots were averaged to reduce the error induced by spatial variability (more details can be found in previous studies [*Oishi et al.*, 2013]). Soil porosity (p) was determined from measured θ near field saturation (θ_s) for each of the five depths. Here p was set as 1.1 times of θ_s derived from all the soil moisture measurements during the period from 2005 to 2006. Soil heat flux (G_s) near the surface ($z = 3$ cm) was measured adjacent to the T_s profiles using soil heat plates (HFT3, Campbell Scientific Inc.). These G_s measurements are used as upper boundary conditions when modeling T_s in the soil. All the aforementioned measurements from an extended dry down period commencing on DOY (day of year) 57 and ending on DOY 110 in 2006 were employed for model purposes (see Figure 2 for the soil moisture levels).

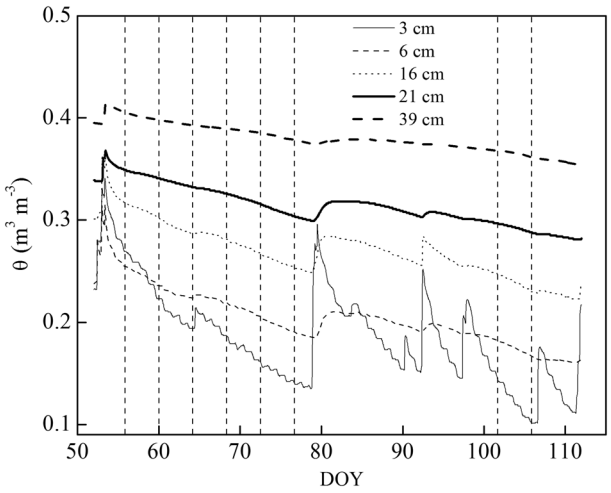

Figure 2. Measured soil moisture series during the selected dry down at various soil depths (from DOY 57 to 110 in 2006). The eight vertical dashed lines denote the eight levels of selected soil wetness used in the model runs as prototypical of various soil moisture states. The commonly used soil moisture shape is the fourth profile (unless otherwise stated).

2.2. The CO_2 Transport Model

To explore the onset of the hysteretic F-T_s and $[CO_2]$-T_s relations at different depths and across a wide range of soil moisture conditions, a one-dimensional CO_2 transport model is employed. The model is based on the continuity equation for gas phase CO_2 given by

$$\frac{\partial f_a[CO_2]}{\partial t} = -\frac{\partial F(z)}{\partial z} + S(z), \qquad (1)$$

where f_a is the air-filled porosity ($f_a = p - \theta$), $F(z)$ is the CO_2 flux at depth z with $F(0) = R_s$ (soil respiration), and $S(z)$ is a local source of CO_2 associated with root and microbial respiration. Because diffusive effects govern CO_2 movement in the soil, the vertical CO_2 flux can be expressed as

$$F(z) = -D(\theta, T_s)\frac{\partial [CO_2]}{\partial z}, \qquad (2)$$

where $D(.)$ is the soil gas phase diffusivity of CO_2 estimated as [*Millington and Quirk*, 1961]

$$D(\theta, T_s) = D_a \left(\frac{T_s + 273}{293}\right)^{1.75} \frac{f_a^{\alpha}}{p^2}, \qquad (3)$$

where D_a (= 0.157 $cm^2\ s^{-1}$) is the free air CO_2 diffusion coefficient at 20°C (i.e., 293 K), and α (= 10/3) is an empirical coefficient determined for this soil type using an independent data set as described in *Suwa et al.* [2004]. Several formulations for the diffusivity-soil-moisture relations are also available, but they share a similar power law behavior, apart from a rather old and seldom used equation by Penman [*Blagodatsky and Smith*, 2012, Figure 3]. Relative differences among formulations may become important near saturation, as models based on a percolation threshold predict zero diffusivity when this air-filled porosity threshold is crossed, whereas the others reach zero diffusivity only at full saturation. The analysis here considers soil moisture values far from saturation, and thus the model runs are all performed in conditions where differences among models are not expected to be large as discussed elsewhere [*Suwa et al.*, 2004]. Therefore, the results for the commonly used Millington and Quirk model are used here with α set to 10/3 as determined from prior experiments at the site.

In all model runs, the top 50 cm of the soil was vertically divided into five layers of dz = 10 cm thickness, with each layer center treated as a computational node (i.e., 5, 15, 25, 35, and 45 cm). As upper boundary condition of the $[CO_2]$ model, the $[CO_2]$ at 0 cm was set to ambient atmospheric conditions (= 380 ppm). The diurnal variation of this upper boundary condition (< 20 ppm) is not likely to affect the outcome appreciably given that the $[CO_2]$ in the first layer exceeds 2000 ppm. The lower boundary condition was treated as a zero flux (i.e., $F(z) = 0$ at $z = 45$ cm).

2.3. The Determination of the Source Term

The soil CO_2 production term depends on several biotic and abiotic factors. To explore these biotic and abiotic controls on the $[CO_2]$-T_s and R_s-T_s hystereses sequentially, a set of calculations is proposed with varying degrees of complexities in representing $S(z, t)$. The simplest representation is given as

$$S(z, t) = S_{ref}(z)e^{b(z)T_s(z,t)}, \qquad (4)$$

where S_{ref} is the base CO_2 production reflecting root density and SOC vertical distribution, and b is a local temperature sensitivity parameter related to the Q_{10} coefficient via $Q_{10} = e^{10b}$.

The simultaneous effects of T_s and θ are considered next using [*Davidson et al.*, 1998]

$$S(z,t) = S_{T_s-\theta}(z) e^{b_{T_s(z)} T_s(z,t) + b_{\theta(z)} \frac{\theta(z,t)}{p(z)}}, \quad (5)$$

where $S_{T_s-\theta}$, b_{T_s}, and b_θ are fitting parameters.

The two different S calculation methods in equations (4) and (5) account for two possible scenarios of soil CO_2 production. In general, soil CO_2 production is temperature dependent provided appropriate soil moisture levels are maintained (equation (4)), while in many field conditions, soil temperature and moisture are both controlling factors of soil CO_2 production (equation (5)) [*Davidson et al.*, 1998].

In addition to T_s and θ, photosynthesis is also suggested to be a factor controlling soil CO_2 production by providing photosynthate for root and rhizospheric respiration. To accommodate this scenario, it is assumed that the temperature sensitivity of CO_2 production remains unchanged (i.e., parameter $b(z)$ in equation (4)), but S_{ref} in equation (4) was further modified to account for the effect of photosynthesis on microbial and root respiration. Temporal patterns (not actual magnitudes) of canopy photosynthesis were surrogated to gross primary productivity (GPP) inferred from eddy covariance measurements collected at the site (see Figure S1 in the supporting information) and a time lag, τ, between soil CO_2 production and photosynthesis was then assumed. Hence, when including photosynthesis, S_{ref} was modified to combine the base line CO_2 production and a rhizosphere component that depends on GPP. The S_{ref} was thus corrected by the rate modifier,

$$\chi = \frac{1}{2}\left[1 + \frac{\mathrm{GPP}(t-\tau)}{\mathrm{GPP}_{max}}\right], \quad (6)$$

where GPP_{max} denotes the maximum of a diurnal GPP series, and the effect of photosynthesis is delayed by τ. The S resulting from photosynthesis is determined by multiplying equations (4) and (6) while keeping $b(z)$ unchanged. Again, the main goal here is to construct possible conditions on S so as to explore the R_s-T_s and $[CO_2]$-T_s hystereses, not the absolute values of S of the long-term data set.

To derive plausible parameters for different methods, the source term S was estimated from measurements of soil $[CO_2]$, T_s, and θ using equation (1). A quadratic function was used to fit the soil $[CO_2]$ profiles only for numerical differentiation purposes [*Daly et al.*, 2009].

The values of S_{ref} and b (equation (4)), $S_{T_s-\theta}$, b_{T_s}, and b_θ (equation (5)) at different depths were optimized using calculated $S(z)$, measured $\theta(z)$ and $T_s(z)$. Negative S inferred within the three days after a rain event were discarded.

2.4. Heat Flow Model

The CO_2 transport model in equation (1) requires the variations in $T_s(z,t)$, which were modeled by combining Fourier's heat conduction law with a heat budget equation given as

$$C_p(\theta)\frac{\partial T_s(z,t)}{\partial t} = \frac{\partial}{\partial z}\left[\lambda(\theta)\frac{\partial T_s(z,t)}{\partial z}\right], \quad (7)$$

where C_p is the soil specific heat capacity and λ is the soil thermal conductivity [*Johansen*, 1975]. The soil volumetric specific heat capacity was expressed as $C_p(\theta) = \theta C_\theta + (1-p)C_s$, neglecting the contribution of air; $C_\theta = 4.18$ J cm^{-3} °C^{-1} and C_s are the water and soil heat capacity with C_s determined as

$$C_s(z) = 0.85\rho_b(z), \quad (8)$$

where ρ_b (g cm^{-3}) is the soil bulk density measured by *Oh and Richter* [2005]. The top 100 cm of the soil was divided into 50 layers of 2 cm thickness with the center of each layer treated as a computational node for numerical calculations of heat flow. Measured subsurface soil heat flux (at $z = 3$ cm) was used as a boundary condition at the surface, and zero heat flux was imposed at the bottom of the 100 cm domain.

2.5. Numerical Runs

A hierarchy of numerical model runs were conducted to determine the onset and magnitude of the hysteretic $[CO_2]$-T_s and F-T_s relations at different z in the absence of space-time variations in soil moisture.

As gas transport and heat flow are both potential factors responsible for the hysteresis, the first set of runs was designed to disentangle them. To achieve this goal, this set of runs is purely hypothetical based

on prescribed soil conditions by assuming that soil texture is vertically uniform with soil porosity set to $p(z) = 0.5\ m^3\ m^{-3}$. Soil temperature was also set vertically uniform (equivalent to assuming $\lambda \to \infty$), and all depths had identical diurnal variations in T_s to investigate the role of gas transport alone in controlling the aforementioned hysteresis. Two scenarios for S are considered: (1) the source term S was set vertically homogeneous with $S(z) = 2\ \mu mol\ m^{-3}\ s^{-1}$ to investigate the onset of hysteresis evolution; (2) $S(z)$ was determined using equation (4) by considering controls of the temporally fluctuating soil temperature but with vertically homogeneous parameters ($S_{ref}(z) = 1\ \mu mol\ m^{-3}\ s^{-1}$, $b(z) = 0.1°C^{-1}$). These values, while arbitrarily set, remain within reasonable ranges when depth integrated to yield R_s. Heat flow was then included to generate soil temperature profiles under finite λ so as to investigate the effects of heat flow on $[CO_2]$-T_s and F-T_s hystereses. The parameters of S were also set vertically homogeneous with $S_{ref}(z) = 1\ \mu mol\ m^{-3}\ s^{-1}$ and $b(z) = 0.1°C^{-1}$. The runs were all conducted under different soil moisture levels but assuming their profiles to be momentarily uniform (i.e., $\theta(z) = 0.1$ to $0.45\ m^3\ m^{-3}$ with increment of $0.05\ m^3\ m^{-3}$).

In the second set of runs, measured $\theta(z)$ for eight contrasting levels (see Figure 2) sampled during the selected dry down period were used as prototypical soil moisture profiles. The two different S calculation methods (i.e., equations (4) and (5)) were then applied, and the parameters were determined as described in section 2.3 (see Figure S2 and Table S1 in the supporting information for details). These runs allow for investigating the hysteretic $[CO_2]$-T_s and F-T_s relations in realistic field conditions where soil wetness impacts simultaneously heat flow and gas movement, but still without plant-derived C.

The third set of runs incorporates the effects of lagged photosynthesis on soil CO_2 production (combining equations (4) and (6)) while maintaining the same $\theta(z)$ profile shape as that in the second set of runs. Because the focus here is on diurnal hysteresis, only subdaily time lags were considered (only $\tau = 0$, 4, 6, and 7 h as typical cases are shown in this study).

To allow the CO_2 transport model to reach "equilibrium," a continuous simulation period of 600 days with 1 min integration time step (= dt) was employed for all runs using concentration measurements at the beginning of the selected period (i.e., DOY = 57) as initial conditions. Note that the soil moisture profiles were unchanged in the first set of runs (i.e., $\theta(z) = 0.1, 0.15, \ldots, 0.45\ m^3\ m^{-3}$). In the second and third sets of runs, the eight levels of soil moisture profiles in Figure 2 were used across the entire simulation period regardless of the natural soil moisture fluctuation, as the purpose is to achieve steady state soil $[CO_2]$ profiles and $F(z)$ in equilibrium with a local soil moisture regime and analyze the hysteresis at this equilibrium soil moisture state. The 600 day period was selected to ensure sufficient integration time to attain equilibration between CO_2 concentration and fluxes and the imposed soil moisture regime for time-varying soil temperature and GPP. All simulations exhibited a near-stationary state in $[CO_2]$ at all layers by the end of the 600 days simulation period. In many cases, $[CO_2]$ exhibited oscillatory but stationary behavior by the end of the simulation period (see Figure S3).

Previous studies investigated the apparent hysteretic relation between R_s (i.e., $F(0)$) and T_s measured at some arbitrary depth (e.g., $z = 2$, 5, 10 cm, etc.). The consequence of this variable choice of a T_s depth on the $F(0)$-T_s hysteresis has been studied and is not elaborated on here. Different from these earlier studies, the focus here is on $F(z)$ (also $[CO_2]$) and $T_s(z)$ hysteresis when colocated at the same depth z. As $F(z)$ is calculated with a model based on CO_2 gradient method, $F(z)$ represents an average flux between two $[CO_2]$ depths, and hence, the corresponding averaged temperature between the two depths was used as the T_s corresponding to $F(z)$.

To obtain temperature variations for the numerical runs of the CO_2 transport model, periodic diurnal soil heat flux series (see Figure S4 in the supporting information) was used to drive T_s for the prescribed soil moisture levels (that are assumed or measured). However, surface temperature variation was applied in the scenario of infinite thermal conductivity (first set). To standardize the soil temperature calculations across scenarios, a uniform soil temperature ($\approx 10.5°C$) was set as initial condition for all heat flow model runs, and a near-stationary state was reached with temperature changing periodically at the end of simulation. The simulation length was set as 10 days, because temperature simulations reach a steady state in a relatively shorter time when compared to gas phase CO_2. Because the thermal conductivity and the specific heat capacity depend on θ, different soil temperature profiles emerged due to different soil moisture levels by the end of model runs.

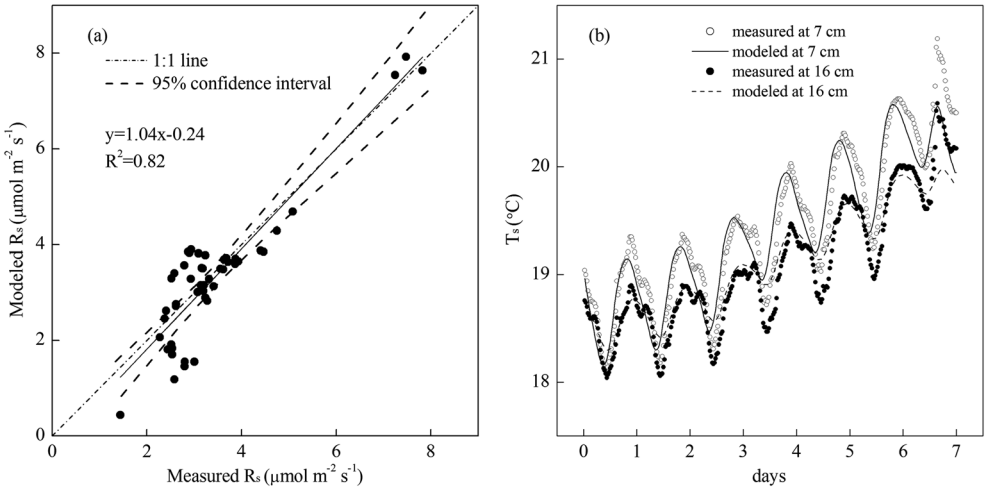

Figure 3. (a) Comparison between measured R_s (i.e., surface CO_2 flux) from soil respiration chambers and modeled surface CO_2 flux by the CO_2 transport model, and (b) comparison between measured and modeled soil temperatures at depths 7 and 16 cm, when using soil thermal parameters described in the text. The coefficient of determination for depths 7, 16, 21, 28, and 38 cm were 0.83, 0.93, 0.89, 0.82, and 0.70, respectively, and the relative RMSEs were 1.6%, 1.1%, 1.4%, 2.3%, and 3.0%, respectively.

3. Results

3.1. Performance of the CO_2 Transport and Heat Flow Models

The CO_2 transport model was tested against field measurements of surface CO_2 flux. The model reasonably captured the independently measured R_s (see Figure 3a) from chambers thereby lending some confidence in its realism for hysteresis analysis at this site. The heat flow calculations also reasonably reproduced soil temperature profiles (see Figure 3b) when the thermal properties of the soil are specified as a function of measured $\theta(z)$. It can be surmised that the model provides reliable soil temperature profiles for the numerical runs employing the CO_2 transport model.

3.2. Hysteresis Driven by Gas Transport and Time Lags in Heat Transport

In the first set of model runs with uniform soil properties, S was set to a constant value across depths and neglected heat flow by assuming an infinite soil thermal conductivity. With this setup, the $[CO_2]$-T_s and F-T_s elliptic clockwise loops were evident (see Figures 4a and 4b at $z = 5$ cm as illustrations). This finding confirms that gas transport alone can produce hysteresis resulting from variations in gas diffusion coefficient in equation (3) induced by diurnal temperature variation. The hysteresis vanished (not shown) when setting $T_s = 20$°C in equation (3) because both $[CO_2]$ and F were constant and temperature variation effects on the diffusion coefficient were suppressed. When S was controlled by temperature as in equation (4), hystereses also emerged (see Figures 4e and 4f), but the directions changed to counterclockwise. When soil thermal conductivity was finite and soil temperature profiles were generated using the heat flow model, the loops in Figures 4i and 4j confirmed that lags due to heat transport alone can introduce $[CO_2]$-T_s and R_s-T_s hystereses as already noted in previous modeling studies [e.g., *Phillips et al.*, 2011]. The dependence of the hysteresis magnitude, determined from the area (A_{hys}) bounded by the elliptic loops (Figure 1d) on θ showed that A_{hys} of $[CO_2]$-T_s correlates positively with θ for all z (Figures 4c, 4g, and 4k) across different scenarios, while the A_{hys} of F-T_s correlates negatively with θ (Figures 4d, 4h, and 4l) regardless of the scenarios. Here the area A_{hys} was used to describe the hysteresis magnitude because it integrates the effects of the two focal points defining the elliptic relation between temperature and either soil respiration or CO_2 concentration.

These A_{hys} results indicate that the hysteretic patterns of $[CO_2]$-T_s and F-T_s have opposite soil moisture dependencies, also consistent with earlier studies and model runs [e.g., *Phillips et al.*, 2011].

3.3. Compound Effects of Temperature and Soil Moisture Profiles on Hysteresis

In the second set of model runs, $S(z)$ was first calculated using equation (4) (with optimized parameters) so that CO_2 source rate only depends on soil temperature, but CO_2 transport also depends on θ through equation (3). Here elliptic loops associated with time lags in heat flow and diffusion time of CO_2 were also apparent. In particular, the hysteresis at $z = 5$ cm occurred for $[CO_2]$-T_s (Figure 5a) and F-T_s (Figure 5b), as examples for one of

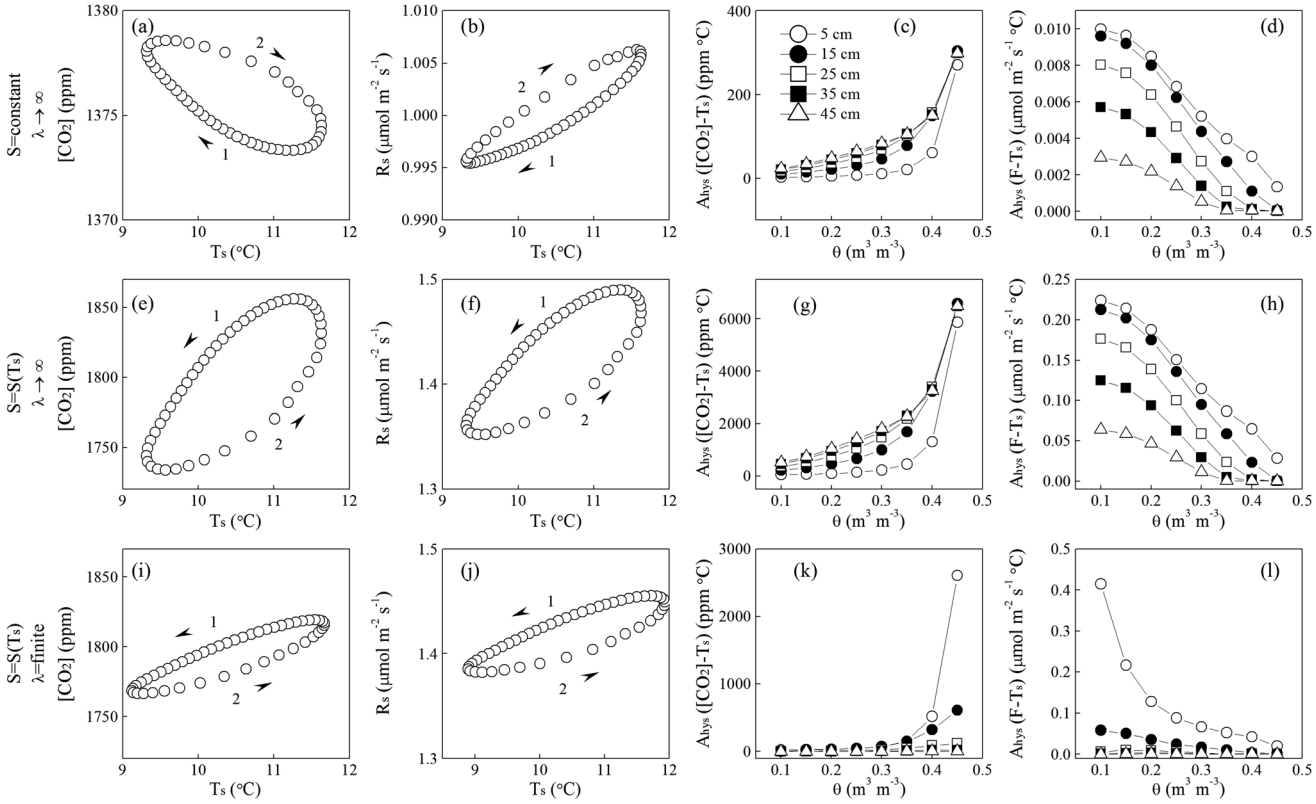

Figure 4. Results of the first set of runs for hysteresis at depth $z = 5$ cm when $\theta(z) = 0.25$ m^3 m^{-3} (shown as example). Soil temperature that is vertically uniform (by assuming an infinite thermal conductivity), with (a) [CO_2]-T_s and (b) R_s-T_s showing relations with constant source term S. (e and f) Runs under temperature-dependent S scenario (i.e., S determined by equation (4)). (i and j) Runs when the soil temperature profile is driven by field measured heat flux subjected to typical field thermal properties and S is temperature-dependent (i.e., S determined by equation (4)). The numbers and arrows indicate the progression during the day, number 1 corresponds to midnight. (c and d), (g and h), and (k and l) Dependencies of the hysteresis area (A_{hys}) on soil moisture for [CO_2]-T_s and F-T_s for the three different scenarios, respectively.

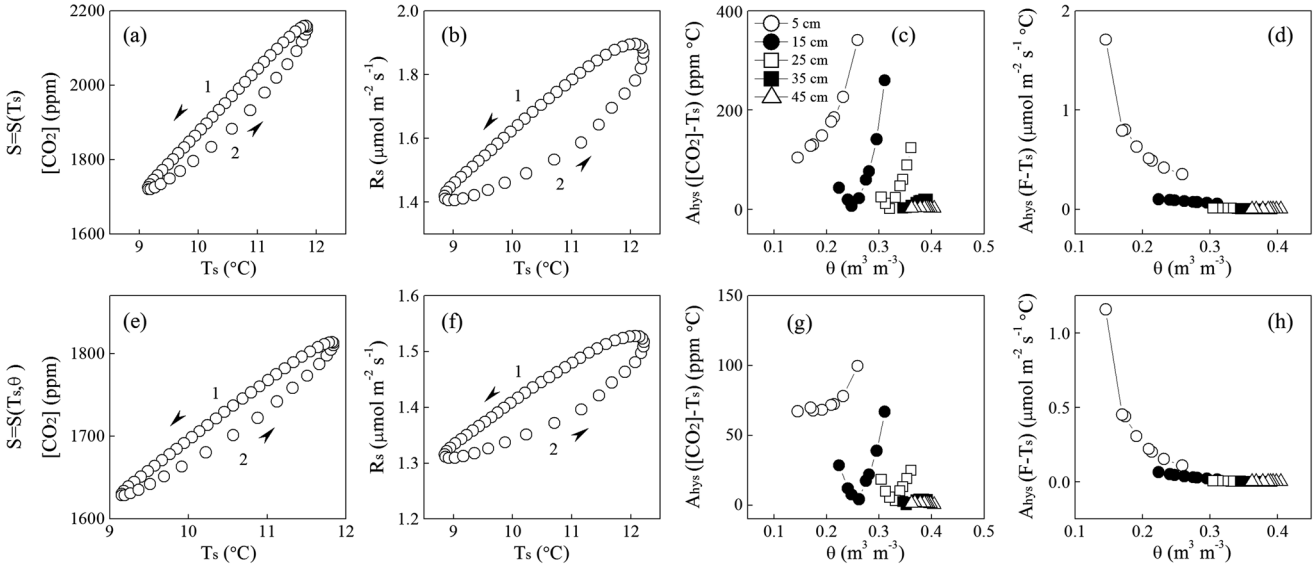

Figure 5. Results of the second set of runs under realistic moisture and temperature field conditions and optimized parameters of the source term S. Hysteresis at $z = 5$ cm are shown as examples for the fourth soil moisture level. (a) [CO_2]-T_s and (b) R_s-T_s relations when S only depends on T_s (equation (4)); (e and f) the same relations as in Figures 5a and 5b when S also depends on θ (equation (5)). The numbers and arrows indicate the progression during the day, number 1 corresponds to midnight. (c and d) The corresponding dependencies of A_{hys} for [CO_2]-T_s and F-T_s on soil moisture at different depths when S is determined by equation (4); (g and h) similar dependencies as in Figures 5c and 5d when S is determined by equation (5).

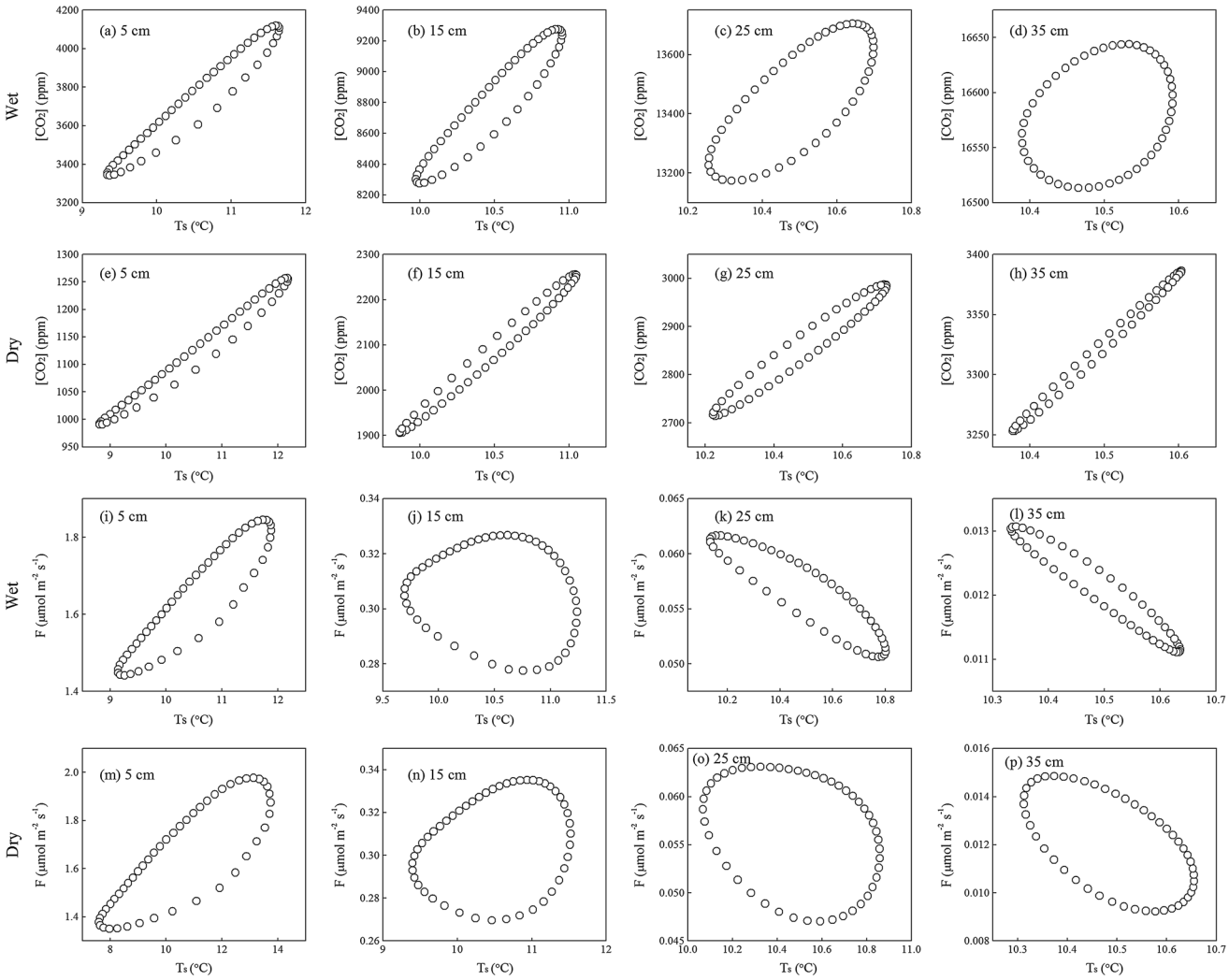

Figure 6. Hysteresis at different depths and soil moisture levels when the source term S only depends on T_s (equation (4)) in the second set of runs. (a–d) and (i–l) $[CO_2]$-T_s and F-T_s hysteresis for the wettest soil conditions (i.e., first soil moisture level in Figure 2); (e–h) and (m–p) those for the driest soil conditions (i.e., eighth soil moisture level in Figure 2). Note that all modeled hysteresis loops exhibit counterclockwise directions.

the $\theta(z)$ profiles (fourth profile shown in Figure 2); other depths had similar loop patterns as shown in Figure 6. The $[CO_2]$-T_s hysteresis exhibited counterclockwise loop patterns at all depths as time progresses (starting at midnight), and $[CO_2]$ correlated positively with T_s. Regarding the $F(z)$-$T_s(z)$ relation, the hysteresis at all z also exhibited counterclockwise loop patterns. However, the correlation patterns appeared to be more complex. The positive F-T_s correlation at $z = 5$ cm gradually degraded and switched to negative with increasing z (e.g., $z = 25$ and 35 cm) (Figures 6k, 6l, 6o, and 6p). At the intermediate $z = 15$ cm, the dependence of $F(z)$ on $T_s(z)$ appeared weak. These results demonstrate that $F(z)$ does not necessarily depend on temperature in a positive manner, especially for intermediate depths where the source term S is low.

Regarding the soil moisture dependence, the hysteretic $[CO_2]$-T_s and F-T_s relations at $z = 5$ cm were similar at different soil moisture levels (Figure 6). Surprisingly, the A_{hys} of $[CO_2]$-T_s did not correlate with θ in a monotonic manner for $z = 15$, 25, and 35 cm, where one soil moisture level corresponded to a minimum A_{hys} (Figure 5c), whereas A_{hys} at $z = 5$ cm correlated positively with θ. Consistent with the first set of runs, A_{hys} of the F-T_s hysteresis correlated negatively with θ in a near-monotonic manner for all z (Figure 5d).

When both T_s and θ were simultaneously accounted for in the source term S calculation using equation (5), the hysteresis loops exhibited similar patterns and orientations (Figures 5e and 5f) as with S determined by equation (4). All the dependence of A_{hys} of $[CO_2]$-T_s on θ at $z = 15$, 25, and 35 cm exhibited a minimum A_{hys} at

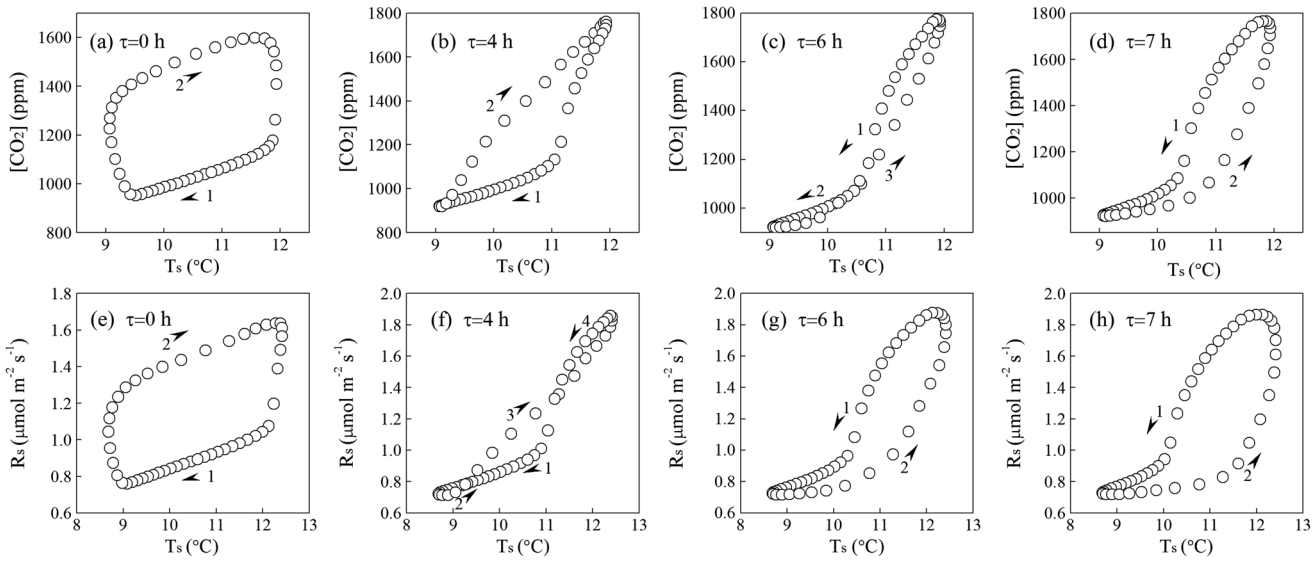

Figure 7. Hysteresis of soil $[CO_2]$ (a–d) and R_s (e–h) with T_s at $z = 5$ cm for the fourth soil moisture level using different subdaily time lags τ between photosynthesis and soil CO_2 production. The numbers and arrows indicate the progression during the day, number 1 corresponds to midnight.

some moisture level (Figure 5g), while A_{hys} for the F-T_s of all depths correlated negatively with θ in a monotonic manner (Figure 5h), consistent with earlier results when S was determined by soil temperature alone.

In summary, the two different S calculation methods result in A_{hys} for F-T_s correlating negatively with increased θ, while the dependence of A_{hys} for $[CO_2]$-T_s on θ is more complicated. There appears to be a regime where A_{hys} achieves a minimum for intermediate θ.

3.4. Compound Effects of Soil Temperature, Moisture, and Photosynthesis on Hysteresis

For the third set of runs, lagged photosynthesis was included in S by combining equations (4) and (6). Here new hysteresis loop patterns emerged for both $[CO_2]$-T_s and R_s-T_s. Altering the time lag τ between CO_2 production and photosynthesis introduced the most dynamically interesting features in the hysteresis patterns for both $[CO_2]$-T_s and R_s-T_s relations (Figure 7). Qualitatively, for $\tau = 7$ h, the outcome of these model runs appeared not too different from the second set of runs in terms of loop shape and direction (see Figures 7d and 7h), respectively). Upon reducing τ, the previously reported loop direction was reversed from counterclockwise to clockwise, and an asymmetric 8-shaped pattern emerged during the transition at an intermediate τ for both $[CO_2]$-T_s and R_s-T_s hysteresis loops (Figures 7c and 7f), where two or more "lobs" appeared in the $[CO_2]$-T_s and R_s-T_s relations.

4. Discussion and Conclusions

While several studies highlighted the presence of hysteretic loops in the soil respiration-temperature and soil CO_2 concentration-temperature relations (Table 1), a unified framework that links all the main drivers for these loops to environmental (soil moisture) and biogeochemical conditions (CO_2 source versus temperature and moisture relations; plant contributions) remains elusive. By sequentially adding contributions to CO_2 production rates and transport, we identified individual and compound drivers of the hysteretic loops. Hysteresis occurs in the absence of vertical profiles of temperature and moisture and for constant CO_2 production rate because daily temperature fluctuations cause a daily cycle in CO_2 transport rate (through thermal effects on gas diffusivity; Figures 4a and 4b). This loop is small and has clockwise direction. When temperature effects on CO_2 production are added, the loop alters direction and gains in magnitude (Figures 4e–4h), but is again reduced when considering delays in temperature changes through the soil profile (Figures 4i–4l). Therefore, temperature may both enhance (through effects on S) and inhibit (when heat conduction is finite) the hysteretic loops. As discussed next, soil moisture effects and plant contributions through photosynthesis further complicate the picture.

On a diurnal basis, soil moisture fluctuations are comparatively small within the root zone and have been discarded as a factor responsible for the R_s-T_s hysteresis by some studies [*Gaumont-Guay et al.*, 2006;

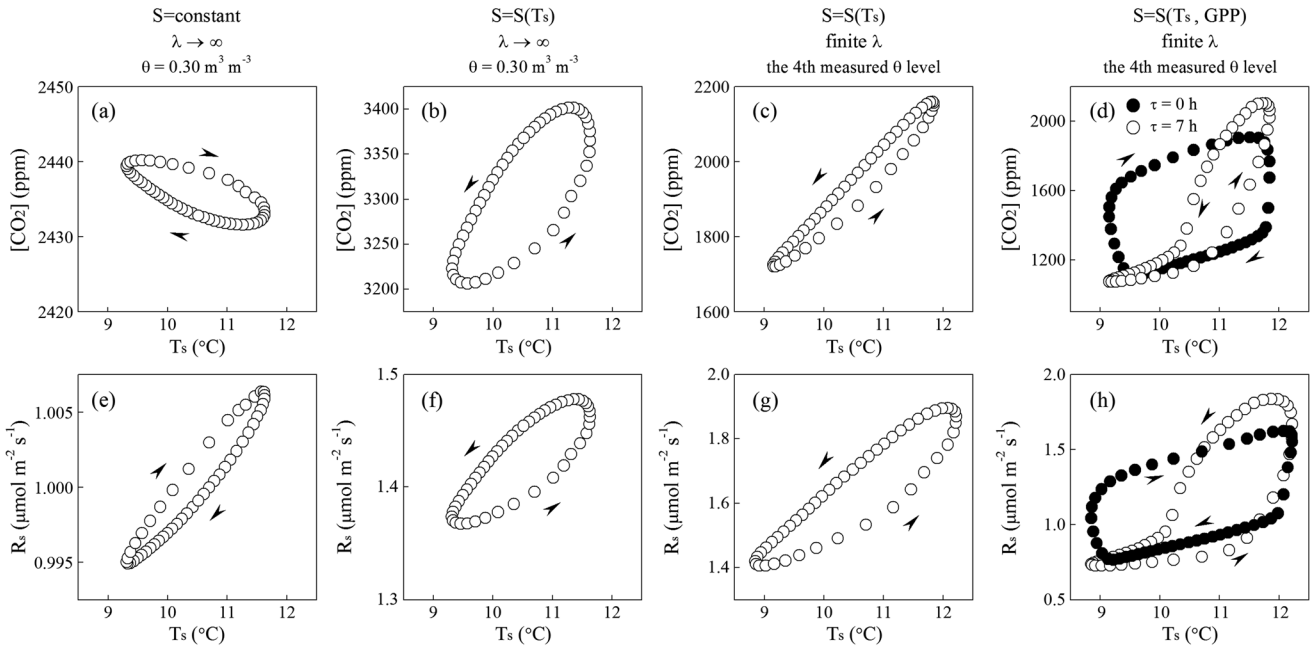

Figure 8. Comparisons of hysteresis loops of soil $[CO_2]$ and R_s with T_s at $z = 5$ cm, across the different numerical runs, (a and e) $[CO_2]$-T_s and R_s-T_s relations when S is set constant, thermal conductivity $\lambda \rightarrow \infty$, and $\theta = 0.30$ m^3 m^{-3} in homogeneous soil; (b and f) S varying with temperature, thermal conductivity $\lambda \rightarrow \infty$, and $\theta = 0.30$ m^3 m^{-3} in homogeneous soil; (c and g) S varying with temperature alone under realistic field conditions with the fourth measured soil moisture level; (d and h) S varying with temperature and GPP under realistic field conditions with the fourth measured soil moisture level. Arrows indicate the progression during the day.

Pingintha et al., 2010]. However, it is evident from the model runs here that small changes in soil moisture can impact the R_s–T_s hysteresis magnitude at a given z (Figures 4d, 4h, and 4l). Regarding the near-surface $[CO_2]$-T_s hysteresis, *Riveros-Iregui et al.* [2007] suggested that higher soil moisture results in hysteresis with larger magnitude (Quantified by the maximum width of the elliptic shape of the hysteresis loop instead of its area as used here). This argument agrees with the model calculations here for near-surface $[CO_2]$ when S is constant or only temperature dependent (Figures 4c, 4g, 4k, and 5c). In this scenario, S is controlled by soil temperature alone, while CO_2 diffusion is mainly controlled by soil moisture. Reductions in CO_2 diffusion coefficient with increased θ enhance CO_2 buildup, thereby causing larger $[CO_2]$-T_s hysteresis. However, soil moisture has a more complicated control on the hysteresis magnitude at intermediate depths (e.g., $z = 15$ and 25 cm in Figure 5c and also Figure 5g). These patterns may also depend on the inverse relation between S and θ in this ecosystem (i.e., $b_\theta < 0$ in equation (5)), which indicates oxygen as limitation to microbial metabolism, rather than moisture limitation as often observed during extended dry downs [*Manzoni et al.*, 2012].

The effects of photosynthesis on soil CO_2 were reported with delays ranging from hours to weeks depending on plant size [*Kuzyakov and Cheng*, 2001; *Stoy et al.*, 2007; *Baldocchi et al.*, 2006; *Detto et al.*, 2012; *Zhang et al.*, 2013]. Therefore, we may expect that even at subdaily scales considered here, photosynthesis might contribute to CO_2 concentration and flux dynamics. Though photosynthesis may not be necessary for producing hysteresis, the model results here suggest that the lag between photosynthesis and S can introduce complex $[CO_2]$-T_s and F-T_s hysteretic patterns, in which the directions of the loops can be reversed under various subdaily time lags. For time lags of the order of 7 h, both $[CO_2]$-T_s and F-T_s hystereses exhibited counterclockwise looping directions with increasing time similar to the field conditions (Figure 1). For time lag of 0 h, the hysteresis directions were clockwise for both $[CO_2]$-T_s and F-T_s hystereses. However, this aforementioned case cannot occur as finite time lags between rhizospheric CO_2 production and photosynthesis must always exist due to photosynthate travel times. At the transition between counterclockwise and clockwise directions at intermediate time lag levels, an asymmetric 8-shaped hysteretic pattern appeared in both $[CO_2]$-T_s and F-T_s (Figures 7c and 7f). Field evidence for this 8-shaped $[CO_2]$-T_s pattern (Figure 1) was noted in previous experiments [*Riveros-Iregui et al.*, 2007]. Likewise, a similar 8-shaped hysteretic R_s-T_s pattern was

also reported in other field studies, [e.g., *Parkin and Kaspar*, 2003; *Bahn et al.*, 2008; *Barron-Gafford et al.*, 2011; *Jia et al.*, 2013].

Interestingly, both clockwise and counterclockwise directions in the R_s-T_s hysteresis pattern were reported in experiments (Table 1). Most reported R_s rates were related to a subsurface T_s at depth z. Hence, some of the reported inconsistencies in loop directions result from differences in soil depths selected when analyzing T_s. Removing such inconsistency (in model runs for R_s and T_s) showed that different S dependence scenarios can result in hysteresis with different directionality. For example, when S is only temperature dependent, the $[CO_2]$-T_s and R_s-T_s hystereses are mostly counterclockwise (Figure 6). The inclusion of lagged photosynthesis as a driver of soil CO_2 production can alter the hysteresis direction. This finding suggests that the time lag between soil CO_2 production and photosynthesis may be indirectly estimated by analyzing simultaneously the hysteresis loop patterns and directions at subdaily time scales. In previous studies (including ours), soil respiration was not separated into its autotrophic and heterotrophic components. Both autotrophic and heterotrophic respiration components exhibit hysteretic responses to T_s [*Savage et al.*, 2013], but these two components may exhibit opposite hysteresis directions. Whether measured hysteresis looping directions may aid in discriminating between autotrophic and heterotrophic dominance on R_s is an interesting question for the future.

Generally, the magnitudes of both $[CO_2]$-T_s and R_s-T_s hysteretic loops are not large because of the small diurnal temperature variation in the forested ecosystem considered here. Using additional model runs, it is shown that amplifying these diurnal temperature variations has a positive effect (not shown) on the magnitude of the hysteresis, consistent with other studies [e.g., *Riveros-Iregui et al.*, 2007].

The numerical experiment setup here provides a "catalog" summary on how different factors contribute to the evolutions of $[CO_2]$-T_s and R_s-T_s hystereses, as illustrated in Figure 8 for the 5 cm depth. In homogeneous soil, when setting S constant and assuming thermal conductivity $\lambda \to \infty$, the $[CO_2]$-T_s hysteresis exhibits clockwise direction with $[CO_2]$ correlating negatively with T_s (Figure 8a), and R_s-T_s also exhibits clockwise direction with R_s correlating with T_s in a positive manner (Figure 8e). These patterns are driven by the diffusion coefficient variations due to diurnal temperature fluctuations. When S varies with T_s following the exponential dependence in equation (4), both $[CO_2]$-T_s and R_s-T_s hystereses exhibit counterclockwise directions, and both $[CO_2]$ and R_s correlate positively with T_s (Figures 8b and 8f); these patterns are similar under realistic field conditions (Figures 8c and 8g). Incorporating the effects of heat flow, temperature, and GPP dependencies of S, different time lag levels of $\tau = 0$ h and $\tau = 7$ h result in hysteresis with different directions and patterns (Figures 8d and 8h). To what extent this summary holds across other sites and ecosystems, and how to improve soil respiration simulation by incorporating the hysteresis mechanisms require further field exploration and model development.

Acknowledgments
The authors thank A. Porporato and E. Ward for valuable discussions, C. Oishi for providing soil surface CO_2 efflux data for model validation, the Editors, C. Phillips and reviewers who provided constructive criticisms. This work was supported in part by the United States Department of Energy (DOE) through the Office of Biological and Environmental Research's (BER) Terrestrial Ecosystem Science(DE-SC0006967) and Terrestrial Processes(DE-FG02-95ER6208) programs, the U.S. Department of Agriculture(2011-67003-30222), the National Science Foundation (NSF-AGS-1102227 and (DEB-1145875/1145649), and the National Natural Science Fund of China for Distinguished Young Scholars (project 51025931). Q. Zhang is supported by China Postdoctoral Science Foundation (project 2015M570662) and foundation for young scholars at Wuhan University (project 206-410500128); Data sets for this paper are available upon request by contacting the corresponding author (Q. Zhang, quan.zhang@whu.edu.cn).

References

Bahn, M., et al. (2008), Soil respiration in European grasslands in relation to climate and assimilate supply, *Ecosystems*, *11*(8), 1352–1367.
Baldocchi, D., J. W. Tang, and L. K. Xu (2006), How switches and lags in biophysical regulators affect spatial-temporal variation of soil respiration in an oak-grass savanna, *J. Geophys. Res.*, *111*, G02008, doi:10.1029/2005JG000063.
Barron-Gafford, G. A., R. L. Scott, G. D. Jenerette, and T. E. Huxman (2011), The relative controls of temperature, soil moisture, and plant functional group on soil CO_2 efflux at diel, seasonal, and annual scales, *J. Geophys. Res.*, *116*, G01023, doi:10.1029/2010JG001442.
Blagodatsky, S., and P. Smith (2012), Soil physics meets soil biology: Towards better mechanistic prediction of greenhouse gas emissions from soil, *Soil Biol. Biochem.*, *47*, 78–92.
Buysse, P., S. Goffin, M. Carnol, S. Malchair, A. Debacq, B. Longdoz, and M. Aubinet (2013), Short-term temperature impact on soil heterotrophic respiration in limed agricultural soil samples, *Biogeochemistry*, *112*(1-3), 441–455.
Carbone, M. S., G. C. Winston, and S. E. Trumbore (2008), Soil respiration in perennial grass and shrub ecosystems: Linking environmental controls with plant and microbial sources on seasonal and diel timescales, *J. Geophys. Res.*, *113*, G02022, doi:10.1029/2007JG000611.
Daly, E., A. C. Oishi, A. Porporato, and G. G. Katul (2008), A stochastic model for daily subsurface CO_2 concentration and related soil respiration, *Adv. Water Res.*, *31*(7), 987–994.
Daly, E., S. Palmroth, P. Stoy, M. Siqueira, A. C. Oishi, J. Y. Juang, R. Oren, A. Porporato, and G. G. Katul (2009), The effects of elevated atmospheric CO_2 and nitrogen amendments on subsurface CO_2 production and concentration dynamics in a maturing pine forest, *Biogeochemistry*, *94*(3), 271–287.
Davidson, E. A., E. Belk, and R. D. Boone (1998), Soil water content and temperature as independent or confounded factors controlling soil respiration in a temperate mixed hardwood forest, *Global Change Biol.*, *4*(2), 217–227.
Davidson, E. A., L. V. Verchot, J. H. Cattanio, I. L. Ackerman, and J. E. M. Carvalho (2000), Effects of soil water content on soil respiration in forests and cattle pastures of eastern Amazonia, *Biogeochemistry*, *48*(1), 53–69.
Detto, M., A. Molini, G. Katul, P. Stoy, S. Palmroth, and D. Baldocchi (2012), Causality and persistence in ecological systems: A nonparametric spectral granger causality approach, *Am. Nat.*, *179*(4), 524–535.
Fu, X. L., M. A. Shao, X. R. Wei, and H. M. Wang (2013), Soil respiration as affected by vegetation types in a semiarid region of China, *Soil Sci. Plant Nutr.*, *59*(5), 715–726.

Gaumont-Guay, D., T. A. Black, T. J. Griffis, A. G. Barr, R. S. Jassal, and Z. Nesic (2006), Interpreting the dependence of soil respiration on soil temperature and water content in a boreal aspen stand, *Agric. For. Meteorol.*, *140*(1-4), 220–235.

Janssens, I. A., et al. (2010), Reduction of forest soil respiration in response to nitrogen deposition, *Nat. Geosci.*, *3*(5), 315–322.

Jia, X., T. S. Zha, B. Wu, Y. Q. Zhang, W. J. Chen, X. P. Wang, H. Q. Yu, and G. M. He (2013), Temperature response of soil respiration in a Chinese pine plantation: Hysteresis and seasonal vs. diel Q_{10}, *Plos One*, *8*(2), E57858, doi:10.1371/journal.pone.005785.

Johansen, O. (1975), Thermal conductivity of soils (in Norwegian), PhD thesis, Univ. of Trondheim, Trondheim, Norway. (English Translation, No. 637, Cold Reg. Res. and Eng. Lab., Hanover, N. H., 1977).

Jones, D. L., and D. V. Murphy (2007), Microbial response time to sugar and amino acid additions to soil, *Soil Biol. Biochem.*, *39*(8), 2178–2182.

Kuzyakov, Y., and W. Cheng (2001), Photosynthesis controls of rhizosphere respiration and organic matter decomposition, *Soil Biol. Biochem.*, *33*(14), 1915–1925.

Li, Z. G., X. J. Wang, R. H. Zhang, J. Zhang, and C. Y. Tian (2011), Contrasting diurnal variations in soil organic carbon decomposition and root respiration due to a hysteresis effect with soil temperature in a Gossypium s. (cotton) plantation, *Plant Soil*, *343*(1-2), 347–355.

Lloyd, J., and J. A. Taylor (1994), On the temperature-dependence of soil respiration, *Funct. Ecol.*, *8*(3), 315–323.

Manzoni, S., J. P. Schimel, and A. Porporato (2012), Responses of soil microbial communities to water stress: Results from a meta-analysis, *Ecology*, *93*(4), 930–938.

Millington, R., and J. P. Quirk (1961), Permeability of porous solids, *Trans. Faraday Soc.*, *57*(8), 1200–1207.

Oh, N.-H., and D. D. Richter (2005), Elemental translocation and loss from three highly weathered soil-bedrock profiles in the southeastern United States, *Geoderma*, *126*(1-2), 5–25.

Oikawa, P. Y., D. A. Grantz, A. Chatterjee, J. E. Eberwein, L. A. Allsman, and G. D. Jenerette (2014), Unifying soil respiration pulses, inhibition, and temperature hysteresis through dynamics of labile soil carbon and O_2, *J. Geophys. Res. Biogeosci.*, *119*, 521–536, doi:10.1002/2013JG002434.

Oishi, A. C., S. Palmroth, J. R. Butnor, K. H. Johnsen, and R. Oren (2013), Spatial and temporal variability of soil CO_2 efflux in three proximate temperate forest ecosystems, *Agric. For. Meteorol.*, *171-172*, 256–269.

Palmroth, S., R. Oren, H. R. McCarthy, K. H. Johnsen, A. C. Finzi, J. R. Butnor, M. G. Ryan, and W. H. Schlesinger (2006), Aboveground sink strength in forests controls the allocation of carbon below ground and its $[CO_2]$-induced enhancement, *Proc. Natl. Acad. Sci. USA*, *103*(51), 19,362–19,367.

Parkin, T. B., and T. C. Kaspar (2003), Temperature controls on diurnal carbon dioxide flux: Implications for estimating soil carbon loss, *Soil Sci. Soc. Am. J.*, *67*(6), 1763–1772.

Phillips, C. L., N. Nickerson, D. Risk, and B. J. Bond (2011), Interpreting diel hysteresis between soil respiration and temperature, *Global Change Biol.*, *17*(1), 515–527.

Phillips, S. C., R. K. Varner, S. Frolking, J. W. Munger, J. L. Bubier, S. C. Wofsy, and P. M. Crill (2010), Interannual, seasonal, and diel variation in soil respiration relative to ecosystem respiration at a wetland to upland slope at Harvard Forest, *J. Geophys. Res.*, *115*, G02019, doi:10.1029/2008JG000858.

Pingintha, N., M. Y. Leclerc, J. P. Beasley, G. S. Zhang, and C. Senthong (2010), Assessment of the soil CO_2 gradient method for soil CO_2 efflux measurements: Comparison of six models in the calculation of the relative gas diffusion coefficient, *Tellus B*, *62*(1), 47–58.

Raich, J. W., and W. H. Schlesinger (1992), The global carbon-dioxide flux in soil respiration and its relationship to vegetation and climate, *Tellus B*, *44*(2), 81–99.

Risk, D., L. Kellman, and H. BeltRami (2002), Carbon dioxide in soil profiles: Production and temperature dependence, *Geophys. Res. Lett.*, *29*(6), 1087, doi:10.1029/2001GL014002.

Riveros-Iregui, D. A., R. E. Emanuel, D. J. Muth, B. L. McGlynn, H. E. Epstein, D. L. Welsch, V. J. Pacific, and J. M. Wraith (2007), Diurnal hysteresis between soil CO_2 and soil temperature is controlled by soil water content, *Geophys. Res. Lett.*, *34*, L17404, doi:10.1029/2007GL030938.

Ruehr, N. K., A. Knohl, and N. Buchmann (2010), Environmental variables controlling soil respiration on diurnal, seasonal and annual time-scales in a mixed mountain forest in Switzerland, *Biogeochemistry*, *98*(1-3), 153–170.

Savage, K., E. A. Davidson, and J. Tang (2013), Diel patterns of autotrophic and heterotrophic respiration among phenological stages, *Global Change Biol.*, *19*(4), 1151–1159.

Stoy, P. C., S. Palmroth, A. C. Oishi, M. B. S. Siqueira, J. Y. Juang, K. A. Novick, E. J. Ward, G. G. Katul, and R. Oren (2007), Are ecosystem carbon inputs and outputs coupled at short time scales? A case study from adjacent pine and hardwood forests using impulse-response analysis, *Plant Cell Environ.*, *30*(6), 700–710.

Subke, J. A., and M. Bahn (2010), On the 'temperature sensitivity' of soil respiration: Can we use the immeasurable to predict the unknown?, *Soil Biol. Biochem.*, *42*(9), 1653–1656.

Suwa, M., G. G. Katul, R. Oren, J. Andrews, J. Pippen, A. Mace, and W. H. Schlesinger (2004), Impact of elevated atmospheric CO_2 on forest floor respiration in a temperate pine forest, *Global Biogeochem. Cycles*, *18*, GB2013, doi:10.1029/2003GB002182.

Tang, J. W., D. D. Baldocchi, and L. Xu (2005), Tree photosynthesis modulates soil respiration on a diurnal time scale, *Global Change Biol.*, *11*(8), 1298–1304.

Thomas, A. D., and S. R. Hoon (2010), Carbon dioxide fluxes from biologically-crusted Kalahari Sands after simulated wetting, *J. Arid. Environ.*, *74*(1), 131–139.

Updegraff, K., S. D. Bridgham, J. Pastor, and P. Weishampel (1998), Hysteresis in the temperature response of carbon dioxide and methane production in peat soils, *Biogeochemistry*, *43*(3), 253–272.

Vargas, R., and M. F. Allen (2008a), Diel patterns of soil respiration in a tropical forest after Hurricane Wilma, *J. Geophys. Res.*, *113*, G03021, doi:10.1029/2007JG000620.

Vargas, R., and M. F. Allen (2008b), Environmental controls and the influence of vegetation type, fine roots and rhizomorphs on diel and seasonal variation in soil respiration, *New Phytol.*, *179*(2), 460–471.

Vargas, R., and M. F. Allen (2008c), Dynamics of fine root, fungal rhizomorphs, and soil respiration in a mixed temperate forest: Integrating sensors and observations, *Vadose Zone J.*, *7*(3), 1055–1064.

Wan, S. Q., and Y. Q. Luo (2003), Substrate regulation of soil respiration in a tallgrass prairie: Results of a clipping and shading experiment, *Global Biogeochem. Cycles*, *17*(2), 1054, doi:10.1029/2002GB001971.

Wang, B., T. S. Zha, X. Jia, B. Wu, Y. Q. Zhang, and S. G. Qin (2014), Soil moisture modifies the response of soil respiration to temperature in a desert shrub ecosystem, *Biogeosciences*, *11*(2), 259–268.

Zanchi, F. B., A. G. C. A. Meesters, M. J. Waterloo, B. Kruijt, J. Kesselmeier, F. J. Luizao, and A. J. Dolman (2014), Soil CO_2 exchange in seven pristine Amazonian rain forest sites in relation to soil temperature, *Agric. For. Meteorol.*, *192*, 96–107.

Zhang, Q., H. M. Lei, and D. W. Yang (2013), Seasonal variations in soil respiration, heterotrophic respiration and autotrophic respiration of a wheat and maize rotation cropland in the North China Plain, *Agric. For. Meteorol.*, *180*, 34–43.